CAPE Variations in the Current Climate and in a Climate Change

BING YE

Department of Earth and Environmental Sciences, Columbia University, New York, New York

ANTHONY D. DEL GENIO

NASA/Goddard Institute for Space Studies, New York, New York

KENNETH K.-W. LO

Science Systems and Applications, Inc., New York, New York

(Manuscript received 12 December 1996, in final form 24 July 1997)

ABSTRACT

Observed variations of convective available potential energy (CAPE) in the current climate provide one useful test of the performance of cumulus parameterizations used in general circulation models (GCMs). It is found that frequency distributions of tropical Pacific CAPE, as well as the dependence of CAPE on surface wet-bulb potential temperature (Θ_w) simulated by the Goddard Institute for Space Studies's GCM, agree well with that observed during the Australian Monsoon Experiment period. CAPE variability in the current climate greatly overestimates climatic changes in basinwide CAPE in the tropical Pacific in response to a 2°C increase in sea surface temperature (SST) in the GCM because of the different physics involved. In the current climate, CAPE variations in space and time are dominated by regional changes in boundary layer temperature and moisture, which in turn are controlled by SST patterns and large-scale motions. Geographical thermodynamic structure variations in the middle and upper troposphere are smaller because of the canceling effects of adiabatic cooling and subsidence warming in the rising and sinking branches of the Walker and Hadley circulations. In a forced equilibrium global climate change, temperature change is fairly well constrained by the change in the moist adiabatic lapse rate and thus the upper troposphere warms to a greater extent than the surface. For this reason, climate change in CAPE is better predicted by assuming that relative humidity remains constant and that the temperature changes according to the moist adiabatic lapse rate change of a parcel with 80% relative humidity lifted from the surface. The moist adiabatic assumption is not symmetrically applicable to a warmer and colder climate: In a warmer regime moist convection determines the tropical temperature structure, but when the climate becomes colder the effect of moist convection diminishes and the large-scale dynamics and radiative processes become relatively important. Although a prediction based on the change in moist adiabat matches the GCM simulation of climate change averaged over the tropical Pacific basin, it does not match the simulation regionally because small changes in the general circulation change the local boundary layer relative humidity by 1%–2%. Thus, the prediction of regional climate change in CAPE is also dependent on subtle changes in the dynamics.

1. Introduction

Predictions of the magnitude and spatial distribution of climate change depend on the parameterization of poorly understood small-scale processes that determine the nature of climate feedbacks and changes in the general circulation. The role of moist convection, which transports heat and moisture vertically, is central to an understanding of climate change, yet doubts persist about the ability of current general circulation models (GCMs) to represent the effects of this process. For a variety of reasons, it is desirable to know whether convection will be stronger or weaker as climate changes. The answer may depend on one's definition of convection ''strength,'' for example, updraft velocity, mass flux, convection depth, or convective heating. But as a first step, it would be useful to validate parameters related to such indices of convection intensity.

A widely used thermodynamic variable associated with convection onset and strength is convective available potential energy (CAPE), which is the vertical integral of parcel buoyancy between the level of free convection and level of neutral buoyancy. Physically, CAPE measures the maximum kinetic energy per unit air mass achievable by the convection of moist air from the subcloud layer, assuming undiluted ascent, and thus gives an upper limit to the cumulus updraft vertical velocity. The relationship between CAPE and convection is qual-

Corresponding author address: Dr. Bing Ye, Department of Earth and Environmental Sciences, Columbia University, 2880 Broadway, New York, NY 10025.
E-mail: pdbxy@valinor.giss.nasa.gov

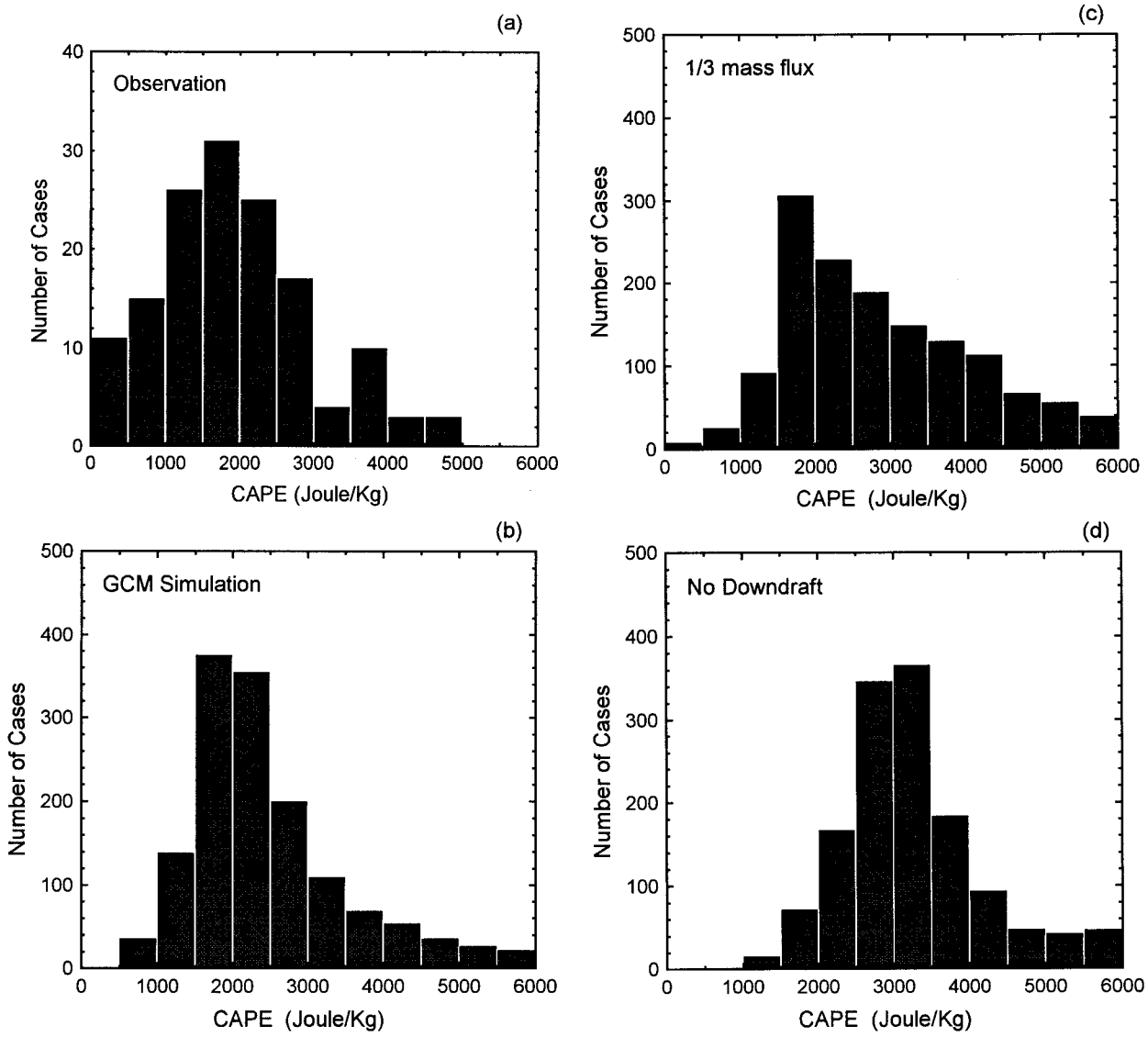

FIG. 1. (a) Observed frequency distribution of CAPE in Darwin, Australia, for pseudoadiabatic ascent from 1000 mb without ice freezing adapted from Williams and Renno (1993). (b) As in (a) but for GCM simulation with complete cumulus parameterization. (c) As in (b) but for convective adjustment time being increased from 1 to 3 h. (d) As in (b) but with convective downdraft eliminated. (e) As in (b) but for parcels lifted from the first GCM layer. (f) As in (e) but CAPE is calculated with reversible moist adiabatic process.

itatively indicated by the positive correlation between observed parcel buoyancies and updraft velocities in oceanic convection, although it apparently cannot explain observed land–ocean differences in cumulus updraft strength (Lucas et al. 1994a,b). Realistic simulation of CAPE variations in a GCM is thus one important test (but not the only one) of the fidelity of its cumulus parameterization's closure assumption and transport mechanisms.

In light of the ability of CAPE to constrain the development of convective systems, questions related to the understanding of the behavior of convection in association with a climate change can be partially addressed by understanding how CAPE changes in a climate change. In this regard, the linear relationship between CAPE and surface wet-bulb potential temperature observed during Australian Monsoon Experiment (AMEX) periods (Williams and Renno 1993) has been interpreted to suggest an increase in CAPE in response to a climate warming due to anthropogenic emission of greenhouse gases; however, whether climate change of CAPE in the real world can be inferred from the patterns of variations in the current climate is unknown. In this paper, we use simulations with the Goddard Institute for Space Studies (GISS) GCM to address the following questions: 1) Why does CAPE vary linearly with surface temperature on short timescales? 2) How does the CAPE–surface temperature relationship vary under dif-

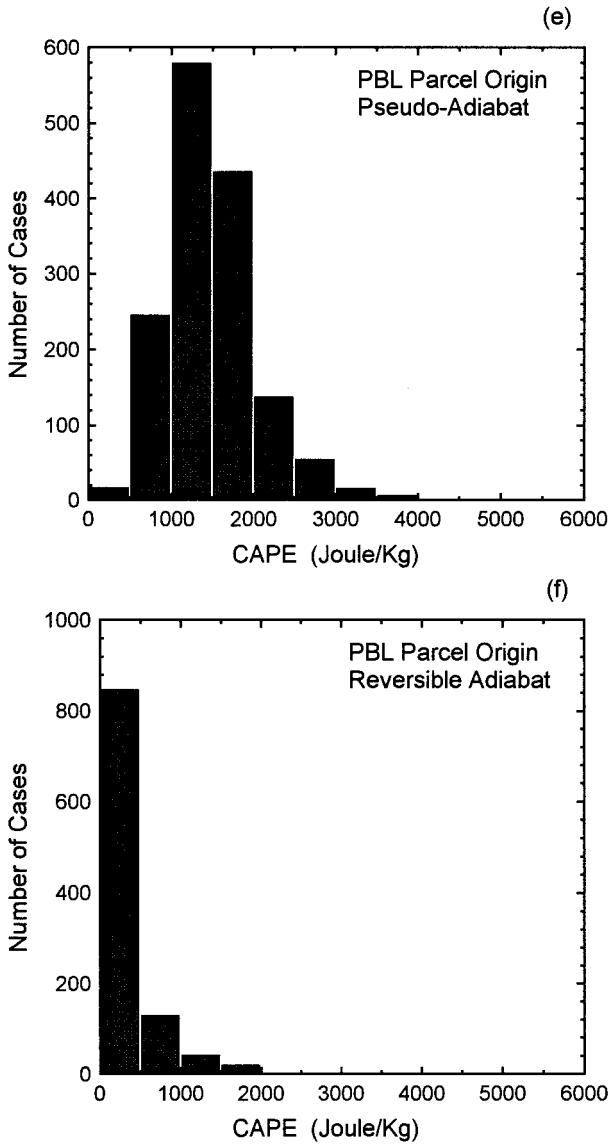

FIG. 1. (*Continued*)

ferent background conditions? 3) Is it possible to predict climate changes in CAPE based on its variability in the current climate? If not, can we use the GCM to develop a way to predict the sign and order of magnitude of climatic CAPE change?

Uncertainty in the estimate of CAPE is associated with the assumption about the microphysical processes taking place when moist air rises. Traditionally, it is assumed that rising cloud parcels follow an irreversible pseudoadiabatic process with the condensed cloud droplets instantaneously falling out of the clouds; this method gives an upper-bound estimate of CAPE. Betts (1982) and Xu and Emanuel (1989) include the effect of all liquid water condensate in determining cloud virtual temperature so that the rising air parcels follow a reversible adiabatic process. The defect of this method is that it is strictly only suitable for nonprecipitating systems, and most tropical cloud clusters precipitate heavily. Williams and Renno (1993) point out that in the mixed phase region ice freezing may release an additional amount of latent heat, which is ordinarily not counted in either of the two other definitions of CAPE. It is interesting that CAPE calculated from the reversible adiabat with ice freezing is comparable in magnitude to CAPE evaluated from the pseudoadiabat. In this study, all three methods for estimating CAPE will be used to understand whether our results are dependent on the microphysical assumption.

The model used in this study is in most respects identical to the model II version of the GISS GCM (Hansen et al. 1983), run at $4^\circ \times 5^\circ$ horizontal resolution with nine vertical levels and a prescribed sea surface temperature (SST). The lowest two GCM levels are located at 959 and 894 mb, respectively; the first model layer is 50 mb thick, comparable to the depth of the tropical oceanic boundary layer. The dynamic time step is 7.5 min and the convective adjustment time is 1 h. The GCM version we use here includes an updated mass flux cumulus parameterization (Del Genio and Yao 1993), a prognostic cloud water budget parameterization for stratiform clouds (Del Genio et al. 1996), and several other changes described in that paper. The GCM uses a cloud-base neutral buoyancy closure assumption, which is sufficient to produce quasi-equilibrium variations of boundary layer relative humidity and tropospheric lapse rate (Yao and Del Genio 1989). The closure assumption determines the mass flux in such a way that after convection the cloud base is restored to be neutrally stable with respect to the next higher level. To simulate the spectrum of cumulus cloud tops, the convection scheme produces two convective plumes for each cloud-base level. The plumes are differentiated by entrainment rate; one is undilute—mimicking a convective core—and the mass flux in the other grows fractionally with height at an entrainment rate of 0.2 km^{-1}. The nonentraining plume receives a fraction of the total cloud-base mass flux given by the large-scale convergence at cloud-base. The convection parameterization includes a representation of convective downdrafts that cool and dry the boundary layer (Del Genio and Yao 1988). For convective events penetrating more than two levels above cloud base, we simply test as the plume rises for the first level at which an evaporatively cooled equal mixture of cloud and environmental air is negatively buoyant. If such a level is found, a downdraft forms there with the properties of the mixture. The downdraft mass flux is specified to be one-third the updraft mass flux. These features suggest that the GISS GCM may be a suitable model for investigating CAPE variations. In all of the results presented from sections 2 to 5, CAPE is computed using the irreversible pseudoadiabatic assumption, unless a specific indication to the contrary is made.

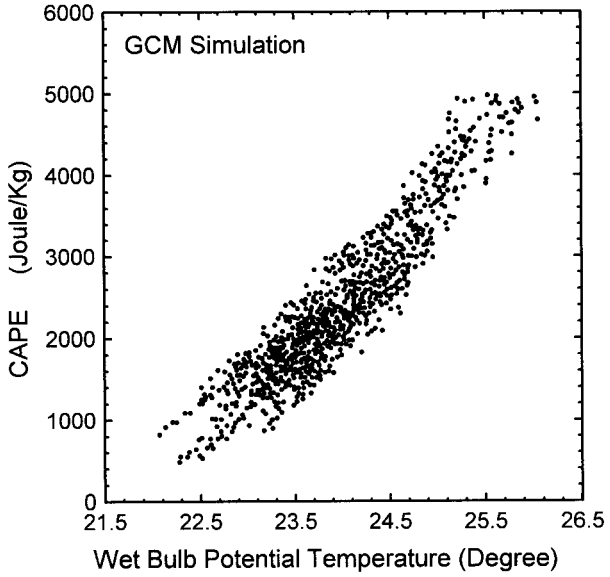

FIG. 2. CAPE (J kg^{-1}) vs Θ_w (°C) simulated by the GISS GCM at Darwin for pseudoadiabatic ascent without ice freezing.

2. Dependence of CAPE on surface wet-bulb potential temperature

CAPE is affected by all physical processes that alter the vertical thermodynamic structure: convection, large-scale dynamics, radiation, and surface fluxes. It is calculated by the following formula:

$$\text{CAPE} = \int_{\text{LFC}}^{\text{LNB}} R_d(T_{\text{vc}} - T_{\text{ve}})\, d\,\text{Ln}P,$$

where T_{ve} and T_{vc} are the virtual temperatures of the environment and cloud parcels lifted from a specified level, respectively; R_d is the gas constant; P is pressure; LFC is the level of free convection; and LNB is the level of neutral buoyancy. Observations from field experiments such as the GARP (Global Atmospheric Research Program) Tropical Atlantic Experiment and AMEX have provided helpful information about the dynamic and thermodynamic structure in tropical convective regions. Analyses of radiosonde data have disclosed a linear relationship between CAPE and surface wet-bulb potential temperature Θ_w in these regions (Williams and Renno 1993). To evaluate the ability of the GISS GCM to simulate the CAPE–Θ_w relationship, hourly temperature and moisture values from the model are produced to compute CAPE and Θ_w. It is found that the GISS GCM produces a frequency distribution of CAPE (assuming for now parcels lifted from the surface, for comparison with the observations) that is quite close to that observed by Williams and Renno at Darwin, Australia, in both mean value and distribution shape (Figs. 1a,b), given the observational uncertainty of approximately 400 J kg^{-1}. The GISS GCM also produces a realistic linear relationship between CAPE and Θ_w in the surface layer (Fig. 2). The GCM simulated mean slope (dCAPE/$d\Theta_w$) in the southwestern tropical Pacific (110°–160°E, 0°–20°S) agrees well with that averaged over the 12 stations sampling the same area in AMEX (Table 1); the difference is within the range of the observational error and the error of the linear regression. Our simulated sensitivity of CAPE to change in Θ_w is also consistent with a recent analysis of Comprehensive Ocean–Atmosphere Data Set and microwave sounding unit data for the global tropical oceans that argues against the concept of ''strict'' quasi-equilibrium (Brown and Bretherton 1997).

TABLE 1. Averaged dCAPE/$d\theta_w$ (J kg^{-1} °C^{-1}) observed among the 12 stations in AMEX (Williams and Renno 1993) and simulated by the GISS GCM in the southwest Pacific (110°E–160°E, 0°–20°S). For observations, E_1 is the error in dCAPE/$d\theta_w$ induced by the random error in measuring CAPE, which is about 400 J kg^{-1} and E_2 is the error due to the scatter of data points in a linear regression.

	Region	dCAPE/$d\theta_w$	E_1	E_2
Observations	12 stations in AMEX	1039	29	19
GCM	110°–160°E, 0°–20°S	1052	0	19

To estimate how sensitive the results are to assumptions inherent in the convection parameterization scheme, we conducted two experiments. In one, the convective adjustment time is increased from 1 to 3 h, which is equivalent to reducing the cumulus mass flux to be one-third of that diagnosed by the closure assumption. This does not cause a significant change in the simulated frequency distribution of CAPE (Fig. 1c), except for a slight increase in the frequency of the highest CAPE events. In another experiment, the convective downdraft is eliminated, and the removal of additional cooling and drying in the boundary layer results in substantially more cases with higher CAPE (Fig. 1d). This suggests that the CAPE distribution is sensitive to the presence or absence of fundamental convective processes in the parameterization but is not strongly influenced by details of uncertain aspects of the parameterization.

Both experiments also reproduced the observed linear relationship between CAPE and the surface wet-bulb potential temperature. The simulated dCAPE/$d\Theta_w$ averaged over grid points corresponding to the 12 stations in AMEX (Williams and Renno 1993) are 1072 J kg^{-1} °C^{-1} and 1091 J kg^{-1} °C^{-1}, respectively, which are only marginally different from that in the control run. The success of the GCM's simulations of the CAPE frequency distribution and the dependence of CAPE on Θ_w in the current climate suggest that CAPE is realistically determined in the GISS GCM in a statistical sense and that simulations of climate change in CAPE may have some degree of credibility. The insensitivity of dCAPE/$d\Theta_w$ to changes in the convective downdraft and cumulus mass flux magnitude indicates that the prediction of climate change in CAPE may not strongly depend on the details of the convection parameterization.

The CAPE values in Figs. 1a,b are somewhat larger

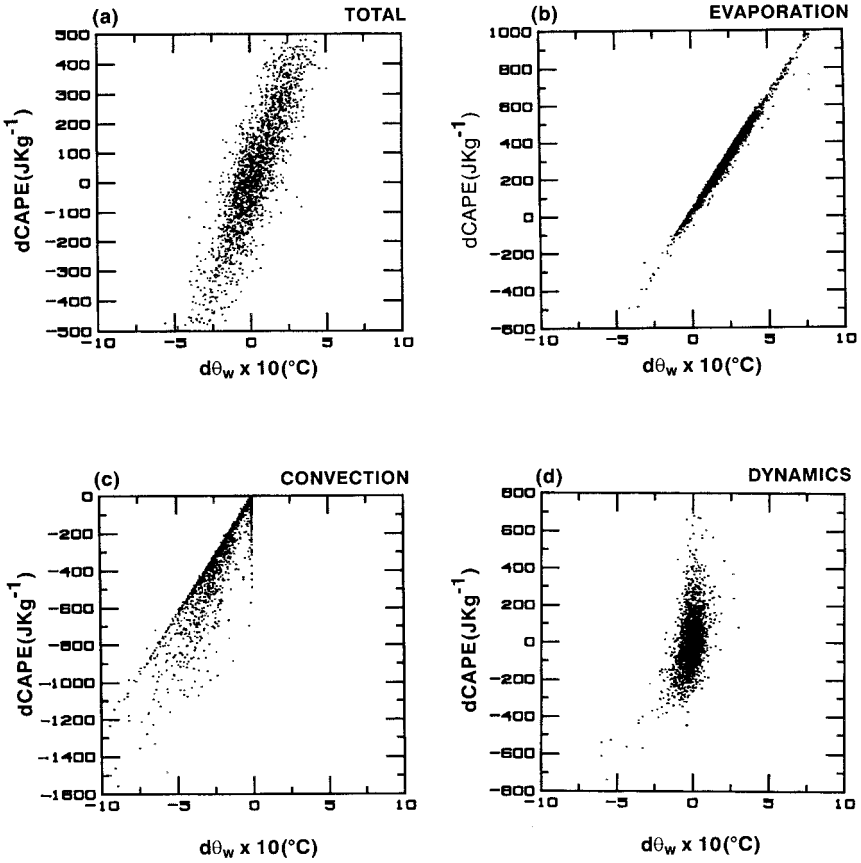

FIG. 3. Change of CAPE (J kg^{-1}) vs change of Θ_w (10^{-1} °C) for each GCM time step (a) due to all the physics, (b) due to surface evaporation only, (c) due to moist convection only, and (d) due to large-scale dynamics only.

than some estimates because parcels are assumed to originate from the surface, where Θ_w is a maximum. In some cases convective parcels originate with the thermodynamic properties of the mixed layer. Figure 1e shows the CAPE distribution simulated by the GCM for parcels lifted from the first model layer (which is actually used by the parameterization to assess instability). The resulting CAPE values are significantly lower. If CAPE is calculated using the reversible moist adiabatic process (Fig. 1f), CAPE values further decrease greatly, and they are more characteristic of the quasi-equilibrium behavior of the model atmosphere. The change of the parcel originating level from surface to the first model layer also decreases the simulated dCAPE/$d\Theta_w$ to about two-thirds of the value calculated by lifting parcels from the surface.

To understand the linear relationship between instantaneous CAPE and Θ_w changes, we use the model to isolate the effect of the most important individual physical processes (e.g., surface evaporation, convection, and large-scale dynamics and compensating subsidence in neighboring grid points; the radiative effect is negligible on short timescales). We partition the total change of CAPE and Θ_w at each physics time step (1 h) into contributions from the individual physical processes and then linearly regress each categorized d-CAPE with the corresponding $d\Theta_w$. Here, the prefix d denotes change due to a certain physical process. Surface Θ_w is only updated once each hour as a result of the cumulative effect of all processes; we therefore use boundary layer (level 1) Θ_w, whose increments due to each process are computed separately, as a proxy to estimate the individual process contributions.

Figure 3a shows the linear relationship involved with all processes in the tropical Pacific (110°–180°E, 26°S–26°N); the linear pattern is similar to that observed in Darwin (Williams and Renno 1993). Figure 3b shows the correlation of dCAPE and $d\Theta_w$ due to surface evaporation; the almost perfect linear relationship and the similarity of the slopes in Figs. 3a and 3b suggest that the part of the linear behavior of the CAPE–Θ_w relationship associated with Θ_w increases primarily originates from the effect of surface evaporation. Sensitivity tests with a fixed typical temperature profile in the Tropics confirm that CAPE varies almost linearly with Θ_w when we modify the moisture content in the boundary layer. This result indicates that at least over the tropical oceans CAPE change is mostly determined by moisture

changes in the boundary layer, while the change in temperature lapse rate may only play a secondary role on very short (<1 h) timescales.

The effect of convection is to dry the boundary layer and heat the free troposphere above it through compensating subsidence in the regions surrounding cumulus updrafts (Yanai et al. 1973) and downdrafts adjacent to the updrafts (Fitzjarrald and Garstang 1981). The drying effect decreases Θ_w, while the warming above the boundary layer increases temperature in the environment of the clouds—that is, both changes of temperature and moisture cooperate to reduce CAPE. This effect of moist convection is shown in Fig. 3c, where almost all points lie in the quadrant with negative values of dCAPE and $d\Theta_w$. A fairly linear relationship between dCAPE and $d\Theta_w$ exists in Fig. 3c, although the linearity is not as good as that related to surface evaporation. Combined with Fig. 3b, it is apparent that the combined effects of evaporation and convection are responsible for the linear behavior in Fig. 3a. The scatter in Fig. 3c occurs because moist convection originates from and detrains at different levels and because convective heating and drying modifies the free troposphere.

The contribution of large-scale dynamics degrades the apparent linear relationship (Fig. 3d). We find that dCAPE and $d\Theta_w$ are almost uncorrelated with each other, and the variability is small in Θ_w but large in CAPE. A possible reason for this behavior is the vertical variation of the large-scale vertical velocity and associated heat and moisture transport. The vertical velocity of the large-scale flow usually increases upward from almost zero near the surface and peaks in the middle troposphere (Thompson et al. 1979). Near the surface, because of the weak vertical motion, the variation of Θ_w due to dynamics is small, while in the middle troposphere large-scale adiabatic cooling or warming controls the lapse rate and thus CAPE.

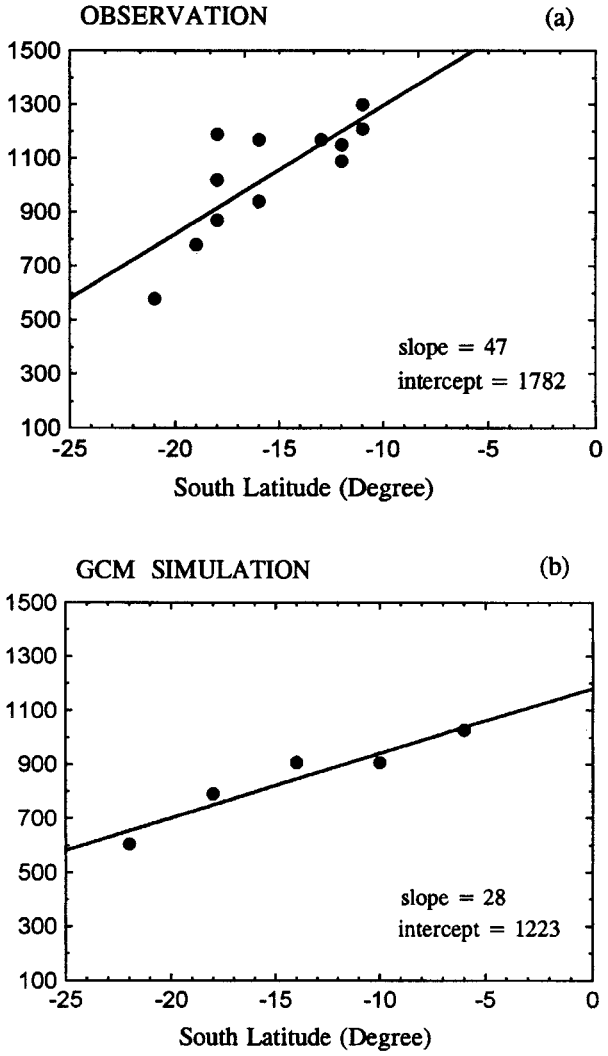

FIG. 4. (a) The dCAPE/$d\Theta_w$ as a function of latitude observed in AMEX, adapted from Williams (1994). (b) The dCAPE/$d\Theta_w$ as a function of latitude simulated by the GISS GCM with the prescribed SST in January 1985.

3. Dependence of the CAPE–Θ_w relation on monthly mean Θ_w

During AMEX, dCAPE/$d\Theta_w$ was also found to decrease away from the equator (Williams 1994) at the rate of 47 J kg^{-1} °C^{-1} lat^{-1} (lat^{-1} denotes per degree in latitude) (Fig. 4a). The GCM simulated change with latitude is about 28 J kg^{-1} °C^{-1} lat^{-1} (Fig. 4b). Considering the errors in regression of 12 J kg^{-1} °C^{-1} lat^{-1} implied in the observations and 4 J kg^{-1} °C^{-1} lat^{-1} in the GCM simulation, the GCM is marginally consistent with the observations. The finite disagreement may be due to either the sparse observational sampling in space or the coarse GCM resolution, which cannot resolve either latitudinal SST variations on scales less than 4° or the detailed structure of the trade inversion in the descending regions of the Hadley and Walker cells.

The spatial variation of dCAPE/$d\Theta_w$ suggests that the relationship between CAPE and Θ_w is not universal in space and time but should instead depend on the mean background conditions. Figures 5a and 5b show the geographical distribution of the zero CAPE intercept Θ_{w0} (the extrapolation of the CAPE–Θ_w regression to zero CAPE) and dCAPE/$d\Theta_w$. Hourly moisture and temperature for each GCM grid in January 1985 are used to perform a linear regression to derive local dCAPE/$d\Theta_w$ and Θ_{w0}. The similarity between their patterns and those of SST and deep convective clouds (Fu et al. 1994) hints at the controlling effects of surface temperature and convection on the variations of CAPE's dependence on Θ_w. Higher zero CAPE intercept values Θ_{w0} are concentrated in the western Pacific (Fig. 5a), which means that boundary layer air must be warmer and wetter more in the western Pacific than in the subtropics or eastern Pacific in order to create conditional instability. This

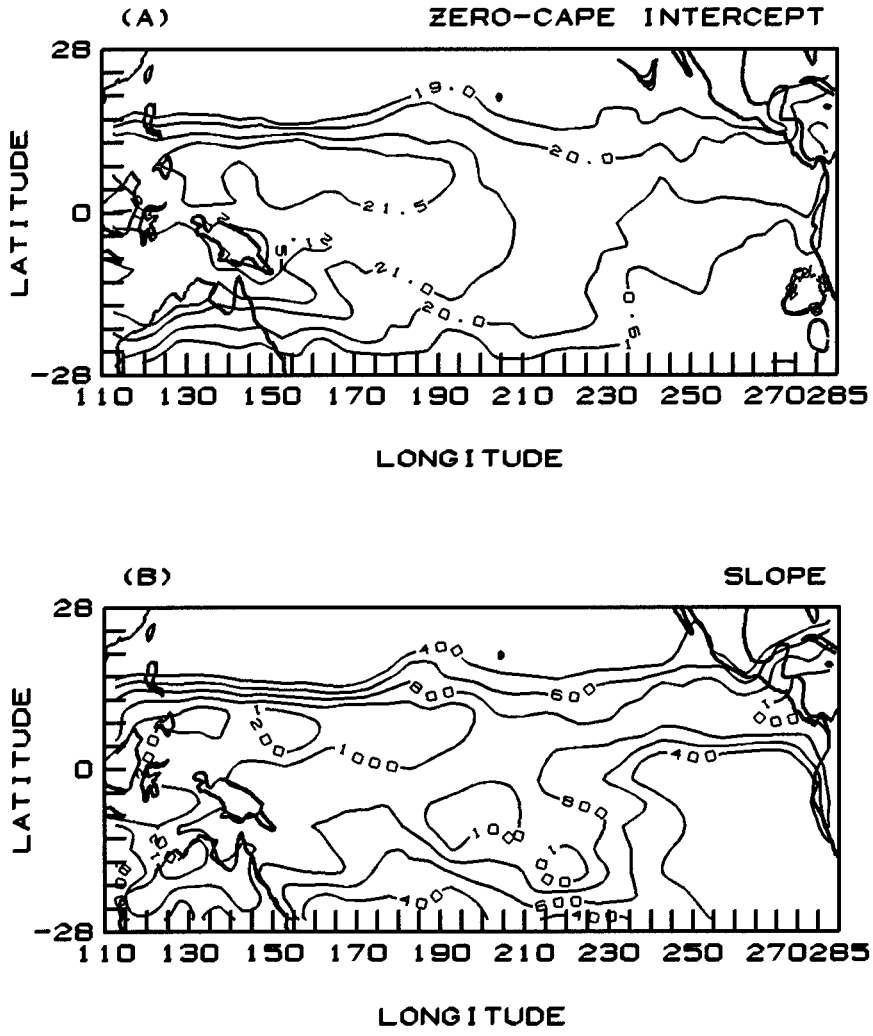

FIG. 5. (a) Geographical distribution of zero CAPE intercept Θ_{w0} (°C) and (b) dCAPE/$d\Theta_w$ (J kg^{-1} °C^{-1}) simulated with the prescribed SST in January 1985.

phenomenon can be understood with the help of a simplified two-layer atmospheric model, which consists of a boundary layer and a trade inversion layer above it. If we use Θ_{1e} and Θ^*_{2e} to denote the equivalent potential temperature and saturated equivalent potential temperature in the first and second layer, respectively, the moist convection instability criterion

$$\Theta_{1e} > \Theta^*_{2e}$$

must be satisfied for CAPE to exist. In a warmer environment like the western Pacific where the temperature in the lower troposphere is higher, there is usually a slightly higher Θ^*_{2e} simply because Θ^*_{2e} monotonically increases with temperature (Fu 1991). Thus, Θ_{1e} has to be higher for the boundary layer to be convective, implying a higher threshold wet-bulb potential temperature Θ_{w0}.

Figure 5b shows that CAPE's sensitivity to Θ_w in a warmer environment is also higher than in a colder one. This is probably associated with the fact that the level of neutral buoyancy (LNB) is systematically lower in the subtropics and eastern Pacific than in the western Pacific because of the cooler SSTs (Fu et al. 1994). Although observations suggest that the level of free convection (LFC) is more variable in space than LNB, the geographical variation of LFC in the GCM is less than that of LNB, probably because of the coarse vertical resolution, which limits our ability to resolve the trade inversion. Since dCAPE is the vertical integral of buoyancy change between the LFC and LNB and geographic variations of parcel buoyancy at different altitudes above the boundary layer are small, the higher vanishing buoyancy level in the warmer environment implies a broader integral range and thus a larger value of dCAPE for the same $d\Theta_w$.

The aforementioned geographic distribution of Θ_{w0} and dCAPE/$d\Theta_w$ simulated by the GCM cannot be fully validated from the observations, but we indeed find that

Θ_{w0} and $d\text{CAPE}/d\Theta_w$ for most stations examined by Williams and Renno (1993) tend to positively correlate with surface temperature. To quantify the correlation simulated by the GCM, we linearly regress $d\text{CAPE}/d\Theta_w$ and Θ_{w0} at each grid point with its local monthly mean surface wet-bulb potential temperature $\overline{\Theta}_w$, where the overbar denotes a monthly average. Model values used in this regression are taken from the tropical Pacific (26°S–26°N, 110°E–75°W) in January 1985. The linear regression yields the fit

$$\Theta_{w0} = 0.78\overline{\Theta}_w + 3.23 \quad \text{and} \tag{1}$$

$$K = 184.0\overline{\Theta}_w - 3281.8, \tag{2}$$

where $K = d\text{CAPE}/d\Theta_w$. The linear correlation coefficients for Θ_{w0} and K are 0.85 and 0.7, respectively. The linear relationship (cf. Fig. 2) between instantaneous CAPE and Θ_w can thus be expressed as

$$\text{CAPE} = K(\overline{\Theta}_w)[\Theta_w - \Theta_{w0}(\overline{\Theta}_w)]. \tag{3}$$

Averaging (3) over time, we obtain the relationship between monthly mean CAPE and Θ_w:

$$\overline{\text{CAPE}} = K(\overline{\Theta}_w)[\overline{\Theta}_w - \Theta_{w0}(\overline{\Theta}_w)]. \tag{4}$$

It is clear from (4) that on the monthly timescale CAPE nonlinearly depends on surface Θ_w.

4. Prediction of climate change in CAPE based on CAPE variability

One possible application of the relationships discussed above is to diagnose the climate change in CAPE. This idea was suggested by Williams (1992) in studying the global electrical circuit. He suggested that since lightning nonlinearly depends on CAPE and CAPE linearly varies with surface temperature, a slight variation in surface temperature can generate a finite response of lightning activity, which can be detected more easily. However, whether the linear relationship observed currently on short timescales can be extrapolated to a climate change timescale is questionable.

The simplest way to predict the change of CAPE in response to a climate change is to assume that the linear relationship between CAPE and Θ_w, which is realistic locally and on short timescales, is valid and uniform in space and time. If we use the observations (Williams and Renno 1993)—that is, $d\text{CAPE}/d\Theta_w = 1000$ J kg^{-1} °C^{-1} and $\Theta_{w0} = 22$°C, a 2°C uniform increase in surface temperature would result in an 1800 J kg^{-1} increase in CAPE (Table 2a), which is equivalent to about a 30 m s^{-1} increase in vertical velocity if the energy conversion efficiency is 100%. This is a dramatic change of convective instability; the atmosphere could not be expected to maintain such an excessive amount of CAPE given the quasi-equilibrium behavior of the current climate (Arakawa and Schubert 1974). If instead we use (4), then when $\overline{\Theta}_w$ increases both $d\text{CAPE}/d\Theta_w$ and Θ_{w0} increase too. The higher value of $d\text{CAPE}/\Theta_w$ leads to a faster increase in $\overline{\text{CAPE}}$ when $\overline{\Theta}_w$ rises, but this trend is counteracted by the increase of Θ_{w0}, which raises the threshold for the production of CAPE and effectively reduces the rate of $\overline{\text{CAPE}}$ increase. Table 2a lists the basinwide CAPE changes in the tropical Pacific derived from this alternative empirical relation and those that were actually realized in a GCM simulation in response to a 2°C increase in SST. It is obvious that even taking into account the temperature dependence of $d\text{CAPE}/d\Theta_w$ and Θ_{w0} based on their geographical variability [Eqs. (1), (2), and (4)], the estimated 1045 J kg^{-1} increase in CAPE is still much larger than the GCM-realized 220 J kg^{-1} increase.

TABLE 2. (a) Climate change in CAPE (J kg^{-1}) for a 2°C increase in SST over the tropical Pacific (110°E–75°W, 26°S–26°N) in July. (b) Climate change in CAPE (J kg^{-1}) for a 2°C decrease in SST over the tropical Pacific (110°E–75°W, 26°S–26°N) in July.

(a) SST+2	
Slope and intercept of CAPE vs θ_w are constant.	1800
Slope and intercept of CAPE vs θ_w are temperature dependent.	1045
[a]Prediction	202
GCM simulation with uniform ΔSST	220
GCM simulation with weakened SST gradient	174
(b) SST−2	
Slope and intercept of CAPE vs θ_w are constant.	−1970
Slope and intercept of CAPE vs θ_w are temperature dependent.	−848
[a]Prediction	−110
GCM simulation with uniform ΔSST	−189
GCM simulation with strengthened SST gradient	−101

[a] CAPE is predicted by assuming constant relative humidity and temperature change according to the temperature change of a parcel with 80% relative humidity lifted from surface.

In the above discussion, CAPE is estimated by raising parcels from the surface. If parcels are lifted from the first model layer, the simulated $d\text{CAPE}/d\Theta_w$ is reduced to about 700 J kg^{-1} °C^{-1} and the predicted CAPE increase for the SST +2 climate (assuming constant slope and intercept) is 1260 J kg^{-1}, which still overestimates the climate change in CAPE. However, the change of parcel originating level hardly changes the prediction of CAPE change realized by the GCM because CAPEs decrease by a similar amount for the different climates in response to the change of parcel origin level. To understand the failure to predict climatic change in CAPE based on its variability in the current climate, consider the variations of thermodynamic properties of the tropical atmosphere in the current climate and in a climate change. In the current climate, CAPE increase on short timescales is either due to an increase of lapse rate because of the concentration of solar heating near the surface or to boundary layer moistening processes (surface evaporation or low-level moisture convergence). In the extreme case that temperature and specific humidity change only in the boundary layer, the sensitivity of CAPE to Θ_w is about 1700 J kg^{-1} °C^{-1} at constant relative humidity. Thus, it is not surprising that

a prediction based on the CAPE–Θ_w relationship on short timescales, which is mostly controlled by surface fluxes in this GCM, results in an overestimated increase in CAPE for a global 2°C rise in SST.

The overprediction of CAPE increase based on the wet-bulb potential temperature dependence of the CAPE versus Θ_w relation also suggests that the geographical variability of CAPE is different from the temporal change of basinwide CAPE on climatic timescales. In the current climate, CAPE differences from one location to another are dominated by differences in boundary layer temperature and moisture, which in turn are controlled largely by SST and large-scale motions (Fu et al. 1994). Thermodynamic structure differences in the middle and upper troposphere are much smaller because the adiabatic cooling and warming in the rising and sinking branches of the Walker and Hadley circulations efficiently smooth out such variations, given the long dissipation time of the tropical atmosphere (Gill 1980). If an approximate seasonal tropical average variability of CAPE is extrapolated to predict climate change in CAPE, a 2°C increase in SST implies an almost 800 J kg^{-1} increase in CAPE (Williams 1994), which is much larger than the GCM-realized climate change CAPE increase but slightly less than that predicted from the geographic variation of CAPE. The seasonal sensitivity of CAPE to Θ_w is roughly estimated by assuming a uniform increase in temperature through the depth of the troposphere (Williams 1994). In this case, the temporal increase of CAPE is mainly due to the increase of SST, which enhances the local evaporation to moisten the boundary layer. Temperature lapse rate hardly changes and thus has little contribution to CAPE change because the seasonal migration of the large-scale circulation acts to suppress temperature variations in the mid- and upper troposphere through adiabatic cooling and warming.

In a forced global climate change, the mean state of the atmosphere evolves from one radiative–convective equilibrium to another, and simulated changes in the Hadley and Walker cells are modest relative to current climate variability. To the extent that the tropical temperature profile is constrained by the moist adiabatic lapse rate (Manabe et al. 1965; Betts 1982; Xu and Emanuel 1989), and the moist adiabatic lapse rate decreases if the atmosphere becomes warmer, the greater warming of the atmosphere with height means that the change of lapse rate has a negative contribution to CAPE change compared to the case with a constant temperature change with height. Thus, the most prominent difference between CAPE change in the current climate and that associated with a climate change lies in the way the lapse rate changes, and because of the negative feedback of lapse rate on CAPE, increase in CAPE in a warmer climate (as realized in the GISS GCM) is much smaller than the prediction inferred from the current climate variability.

In view of the failure of the empirical relationship between CAPE and Θ_w in the current climate to predict climatic change in CAPE, we assume instead that the temperature change between two different climate regimes is according to the moist adiabatic lapse rate change as a consequence of quasi-equilibrium. Our algorithm to predict the CAPE in a warmer/colder climate is defined as follows.

1) Surface temperatures in the current and warmer/colder climates are used and 80% surface relative humidity is assumed to compute vertical profiles of temperature in each climate by raising parcels from the surface. Above the lifting condensation level, the parcels follow the reversible moist adiabat. The difference between the parcel temperatures is computed.
2) Assuming that the temperature change from the current climate to the warmer/colder climate is equal to the parcel temperature difference computed in step 1, we add this difference to the temperature of the current climate at each level to get the temperature profile approximation for the changed climate.
3) Steps 1 and 2 are applied only up to 300 mb. Above this level, temperature change is less than that predicted from the moist adiabat because in this GCM the cumulus mass flux decreases significantly above 300 mb and thus does not control temperature to the same extent. For simplicity, temperature change above 300 mb is assumed to equal that at 300 mb; this is a good approximation to the temperature change realized by the GCM at these levels.
4) A surprising feature of the tropical maritime water vapor distribution in the GCM is that while the absolute water vapor amount varies significantly in the atmosphere, relative humidity remains fairly constant on climatic timescales. Especially in the boundary layer, model results consistently indicate that relative humidity does not vary significantly in response to temperature changes of a few degrees (Betts and Ridgway 1989; Del Genio et al. 1991); this is consistent with observations (Oort 1983; Rind et al. 1991). Thus, we assume that relative humidity is invariant and the problem of predicting CAPE change is thus simplified to predicting temperature variation in a climate change. Later we will show that the neglect of relative humidity change causes a certain amount of error in predicting local CAPE changes, but that the assumption works well on the scale of the Hadley cell.

To test the accuracy of our CAPE prediction, we compare a GCM perpetual July simulation of the current climate with perturbation experiments in which globally uniform SST increases and decreases of 2°C are imposed. Figure 6a shows the predicted buoyancy profile for the SST +2 climate averaged over the tropical Pacific (26°S–26°N, 110°E–75°W); we find that the prediction agrees well with that simulated by the model. Figure 6b shows that predicted monthly CAPE agrees well with simulated CAPE in individual grid boxes.

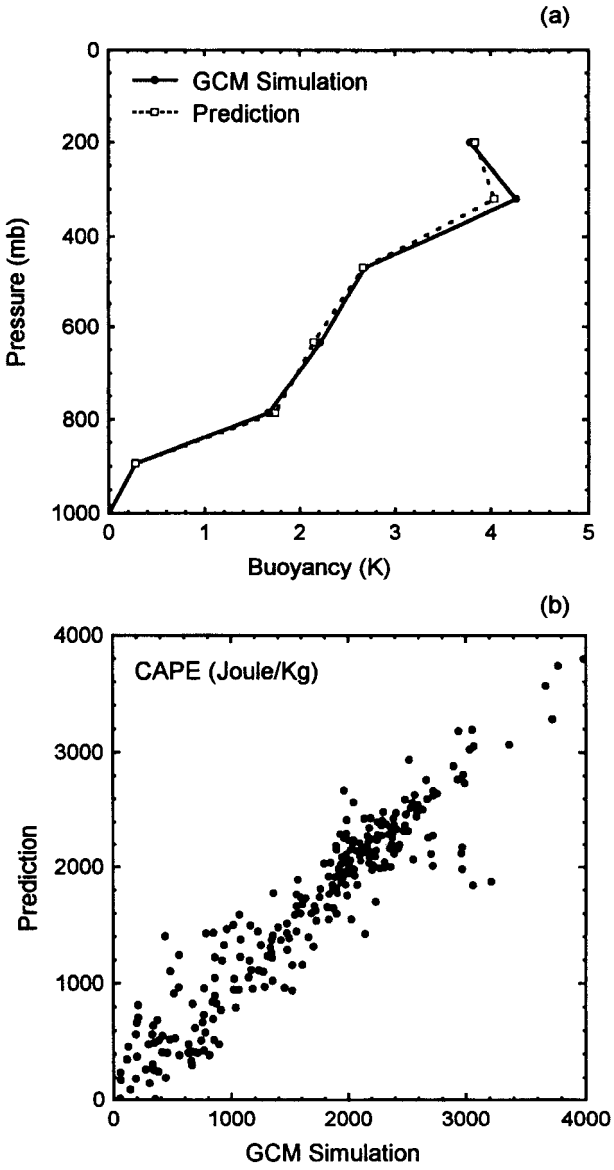

FIG. 6. (a) July monthly mean vertical profiles of parcel buoyancy simulated (solid line) and predicted (dashed line) during deep convection in the tropical Pacific (110°E–75°W, 26°S–26°N) for the SST +2 climate. (b) Predicted July monthly mean CAPE (J kg^{-1}) in the tropical Pacific vs July monthly mean CAPE (J kg^{-1}) simulated by the GISS GCM at individual grid points for the SST +2 climate.

Figure 7a shows the mean buoyancy changes over the tropical Pacific predicted and simulated for the SST +2 climate relative to the current climate. Relative to the buoyancy in the current climate, that realized by the GCM in the SST +2 climate increases little below 300 mb because the temperature change approximately follows the moist adiabatic lapse rate and thus no additional buoyancy is realized by an adiabatically rising parcel. The maximum increase at 200 mb occurs because convective cloud-top height increases in the warmer climate as a result of warmer surface air and a higher LNB. The increase of cloud height is largely determined by the increase of saturation specific humidity in a warmer climate; the decrease of the moist adiabatic lapse rate tends to depress cloud top, but its effect is dominated by the change in humidity (Del Genio 1993).

In Fig. 7b the GCM simulated buoyancy change in the SST +2 climate is partitioned into contributions from parcel temperature change relative to that achieved by lifting the environmental air with the assumed 80% relative humidity, the change in the virtual effect of moist air and a residual due to other processes. The contribution from parcel temperature change is slightly negative because the parcel's relative humidity is slightly less than 80% at the surface and thus its lifting condensation level is higher and colder than that of environmental air with 80% relative humidity. The contribution of the virtual effect is positive as a result of warmer and wetter near-surface air in the SST +2 climate. The positive residual contribution is from enhanced radiative and evaporative cooling, changes in relative humidity and dry convection, and deviations of parameterized moist convection from purely moist adiabatic behavior.

To further quantify nonconvective effects, we start from the energy budget equation to derive an expression for changes in lapse rate:

$$\frac{\partial T}{\partial t} = -\mathbf{V}\cdot\nabla_h T - \omega\frac{\partial T}{\partial p} + \frac{\omega\alpha}{C_p} + Q - E - R. \quad (5)$$

In (5) Q, E, and R represent condensation heating, evaporative cooling, and radiative cooling, respectively, and the other symbols have their conventional meanings. Since temperature tendency and large-scale horizontal advection are negligible in the Tropics, if the equation is averaged over time and the basinwide area, the equation reduces to

$$\frac{\partial T}{\partial p} \cong \frac{1}{\omega}(Q - E - R) + \frac{\alpha}{C_p}. \quad (6)$$

We let Γ denote the lapse rate dT/dp and differentiate the above equation to see the effect of a climate change, giving

$$\frac{d\Gamma}{d\mathrm{SST}} = \frac{1}{\omega}\frac{d(Q - E - R)}{d\mathrm{SST}} - (Q - E - R)\frac{d\omega}{\omega^2 d\mathrm{SST}} + \frac{d\alpha}{C_p d\mathrm{SST}}. \quad (7)$$

For the GCM SST +2 climate change the second and third terms on the right-hand side, averaged over the tropical Pacific and a climatic timescale, are almost an order of magnitude smaller than the first term in the mid- and upper troposphere (Table 3). Thus, lapse rate change on large time- and space scales is mainly determined by changes in diabatic heating. In the tropical convergence region where upward motion implies negative ω, more convective heating will result in a less

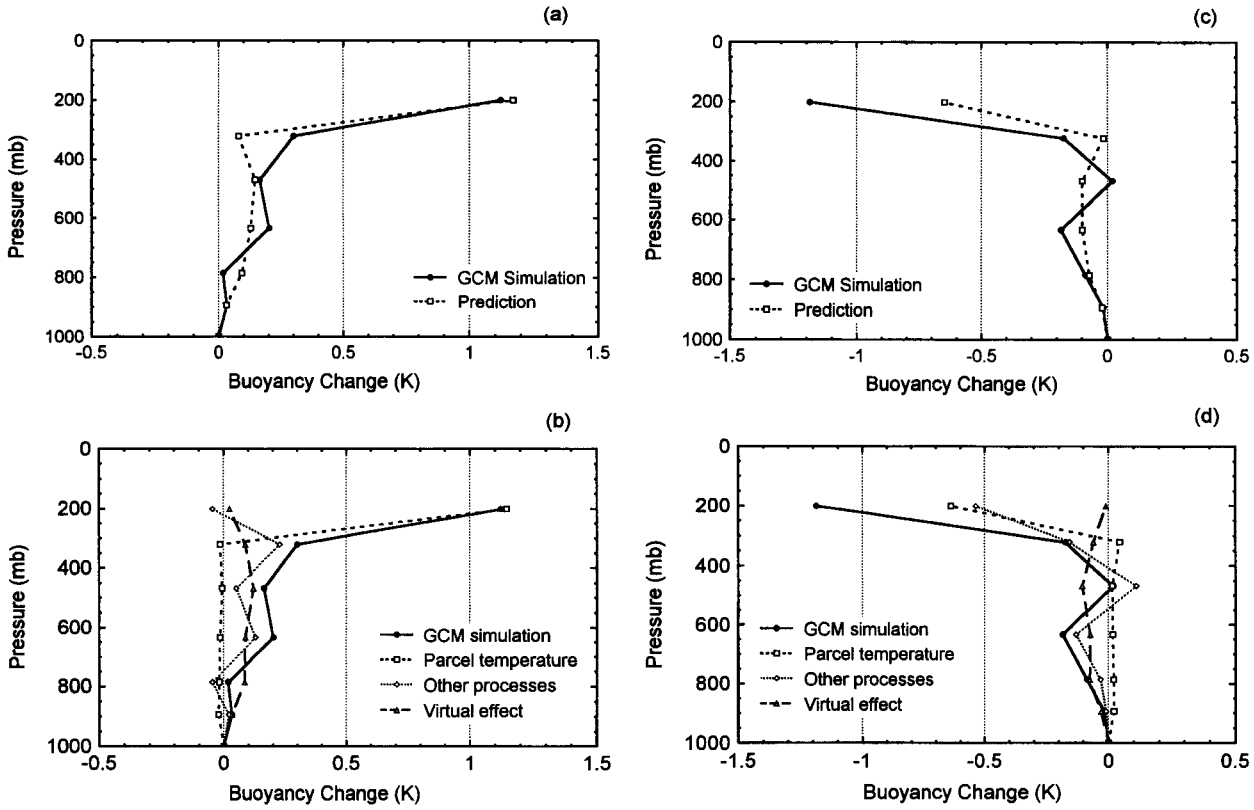

FIG. 7. (a) Changes in the vertical profiles of July monthly mean buoyancy during convection in the tropical Pacific (110°E–75°W, 26°S–26°N) for the SST +2 climate. The GISS GCM simulation is denoted by the solid line; the dashed line is for the prediction. (b) The vertical profile of July monthly mean buoyancy change as shown in (a) simulated by the GISS GCM in the SST +2 climate (solid line) is partitioned into different parts due to parcel temperature change (short dashed line with square), change in virtual effect (long dashed line with triangle), and changes in other processes (dotted line with diamond). (c) As in (a) but for the SST −2 climate. (d) As in (b) but for the SST −2 climate.

steep temperature lapse rate, and more radiative and evaporative cooling will produce a steeper lapse rate. Examination of the energy budgets shows that convective heating, evaporative cooling, and radiative cooling are all enhanced in the SST +2 climate (Table 4). Thus, if radiative and evaporative cooling (about 30% of convective heating) are included, the lapse rate should be steeper than what is predicted from the moist adiabatic assumption. Consequently, the predicted CAPE increase for the SST +2 climate is slightly less than what is actually simulated (Fig. 7a). Note that the balance in Table 3 is very different from that which occurs in general on synoptic time- or space scales; on such scales, changes in vertical motion are large enough to offset the effects of diabatic heating changes—that is, the second term in (7) is of leading order, and horizontal advection may play a role as well.

We also used the same method to predict CAPE change in response to a 2°C decrease in SST. The aforementioned method is unable to predict the correct buoyancy change in the upper troposphere (Fig. 7c), and the predicted CAPE decrease is much smaller than the GCM-simulated CAPE decrease (Table 2b). The reason is that temperature structure is controlled less by moist convection in a colder climate than in a warmer climate. To understand why the prediction overestimates the simulated lapse rate in the SST −2 climate, note that latent heat release is smaller in a colder and drier climate, the result being that dynamic heating terms in (7) become

TABLE 3. Contributions of individual terms on the rhs of (7) to the lapse rate change at 321 mb over the tropical Pacific (26°S–26°N, 110°E–75°W) in July. (Unit: $\times 10^{-3}$ °C mb^{-1})

	$d(Q - E - R)/\omega$	$-(Q - E - R)\, d\omega/\omega^2$	$d\alpha/C_p$
SST +2	−19.0	0.4	4.3
SST −2	7.6	−2.1	−4.1

TABLE 4. Changes in convective heating and radiative and evaporative cooling averaged between 786 and 201 mb over the tropical Pacific (110°E–75°W, 26°S–26°N) in July. (Unit: °C day^{-1}.)

	dQ	dE	dR	$dR/d(Q + E)$
SST +2 − current	0.39	0.05	0.08	23%
SST −2 − current	−0.17	−0.02	−0.08	53%

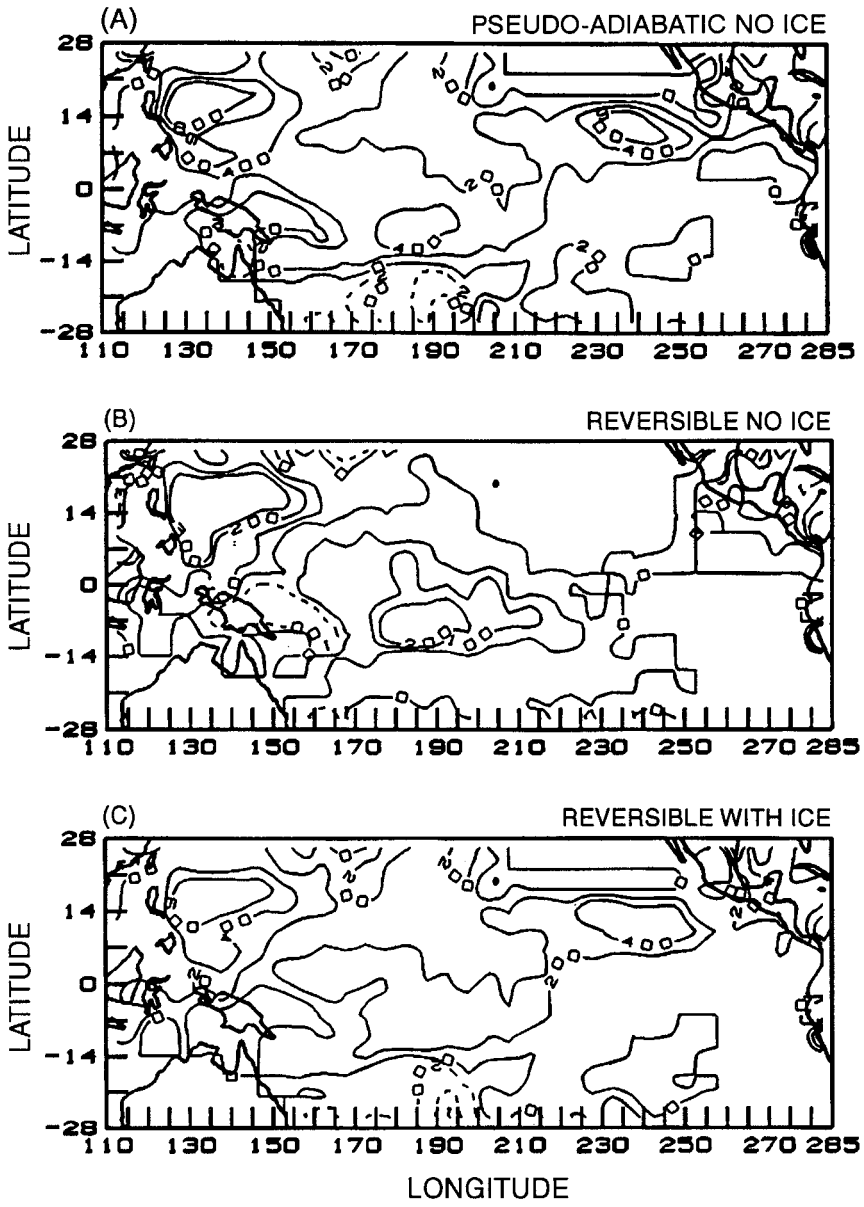

FIG. 8. Geographical distributions of CAPE change (J kg^{-1}) in July for the SST +2 climate simulated by the GISS GCM in response to a uniform 2°C increase in SST. CAPE is computed from three different microphysical assumptions: (a) pseudoadiabatic ascent without ice freezing, (b) reversible ascent without ice freezing, and (c) reversible ascent with ice freezing when temperature is below −10°C.

comparable to the diabatic heating term (Table 3) in determining lapse rate change. In the tropical convergence region, the second and third terms in (7) represent the contributions from the change of large-scale adiabatic cooling due to the change in vertical motion and thermal expansion. Weakened adiabatic cooling in the SST −2 climate decreases lapse rate and thus opposes the increasing lapse rate tendency due to the decreasing convective heating. This result suggests that the moist adiabatic assumption is not symmetrically applicable to a warmer and colder climate. In a warmer regime moist convection primarily determines the temperature structure, but when the climate becomes colder the effect of moist convection diminishes, while the large-scale dynamics becomes relatively important. Furthermore, changes in radiative cooling, which are of comparable magnitude but opposite sign in a warmer/colder climate, make up a larger fraction of the total diabatic heating change in the cooler climate (Table 4).

Figure 8 shows the geographical distributions of simulated changes of CAPE for the SST +2 climate relative to the current climate. To test whether the sign of the

change depends on water loading and condensate phase, we compute CAPE using three different microphysical assumptions about the role of liquid condensate in cloud virtual temperature—that is, that the parcel follows a pseudoadiabat without ice, a reversible moist adiabat without ice and a reversible moist adiabat with ice freezing when the temperature is below −10°C. With the first and the third assumptions, CAPE increases by almost 200 J kg^{-1} in most regions, and it increases by more than 100 J kg^{-1} with the second assumption. Lifting the parcel from the planetary boundary layer (PBL) instead of from the surface gives similar results. This suggests that no matter what definition of CAPE is used, the environment of a warmer climate is slightly more unstable than that of the current climate. In terms of cumulus intensity, the CAPE increases estimated above would result in a 10%–15% increase in the updraft velocity of an undilute parcel.

Figure 9 shows scatterplots of predicted and simulated CAPE change (*d*CAPE) at each individual grid point under different microphysical assumptions. It is obvious that although the predicted basinwide CAPE change agrees well with the GCM simulation (Table 2a), our scheme cannot predict correct local CAPE changes. One common feature in these figures is that the GCM-realized CAPE changes vary greatly among different locations, whereas the predicted CAPE changes concentrate around a narrow range. The most important cause of the lack of spatial variability in predicted *d*CAPE is our constant relative humidity assumption, which neglects 1%–2% relative humidity changes in the boundary layer that occur in the GCM in response to small changes in the tropical general circulation as the climate changes. To quantify this error, we recalculate our CAPE prediction in the SST +2 climate using the actual relative humidity change at each grid point, while temperature change is still obtained from the moist adiabatic assumption. Figure 10a shows that when the actual relative humidity change is used, *d*CAPE can be fairly well predicted in both its basinwide mean and the spatial distribution. We also computed CAPE changes with the actual temperature change in the SST +2 climate and the relative humidity in the current climate; the situation is only slightly improved, which indicates that the moist adiabatic lapse rate assumption is fairly reliable in the Tropics. Correlations between boundary layer relative humidity, surface convergence, and evaporation suggest that the 1%–2% changes in local relative humidity are more closely related to the change in surface convergence (Figs. 10b,c). This suggests that the spatial variability of CAPE change is primarily dynamics driven; surface evaporation is the ultimate moisture source, but it does not directly control the local moisture change in most regions.

The effects of dynamics on CAPE change depend on scale. If one is only interested in the global mean change of CAPE, the effect of dynamics is reduced since the averaged moisture convergence disappears and the thermodynamic conditions are mainly determined by radiative–convective equilibrium. If one's interest lies in the tropical regions, motions on the scale of the Hadley and Walker circulations should be taken into account. To see the scale dependence of the prediction, we averaged temperature and moisture profiles on different horizon-

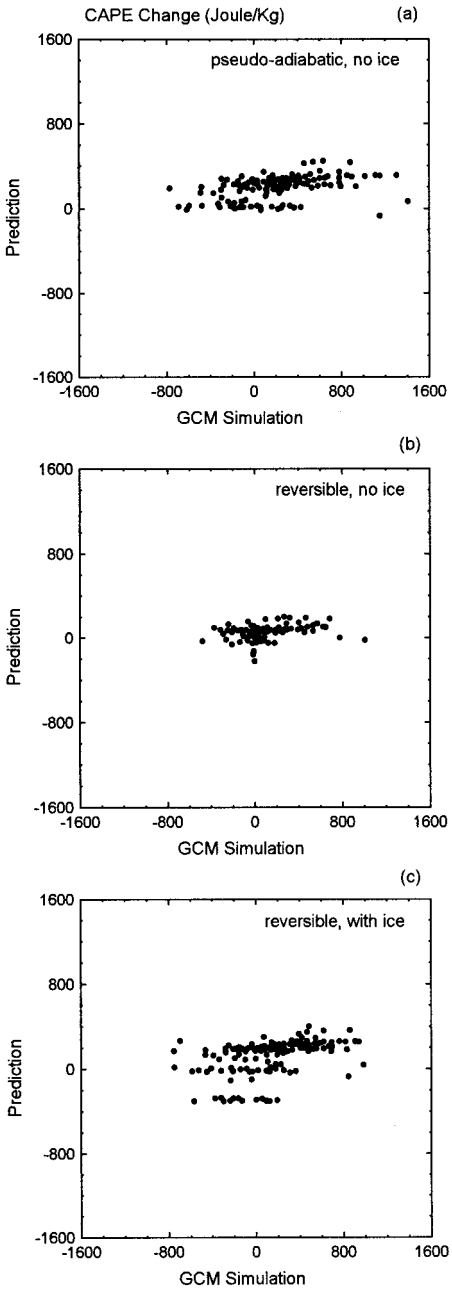

FIG. 9. Scatterplots of changes of CAPE (J kg^{-1}) during deep convection over the tropical Pacific (110°E–75°W, 26°S–26°N) on the scale of 4° × 5° simulated by the GISS GCM against prediction. CAPE changes are computed for July convection events in the current and SST +2 climates: (a) pseudoadiabatic without ice, (b) reversible without ice, and (c) reversible with ice freezing when temperature is below −10°C.

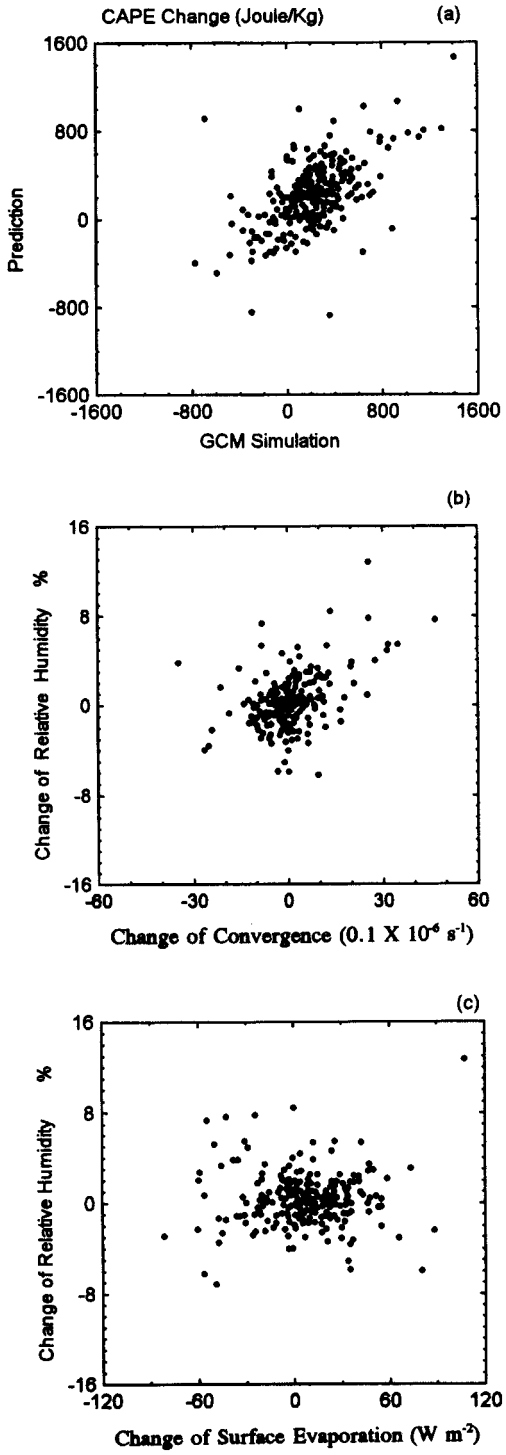

FIG. 10. (a) As in Fig. 9a except that the actual relative humidity in the SST +2 climate is used in the prediction of CAPE. (b) Changes in surface relative humidity (%) vs changes in surface convergence (0.1×10^{-6} s^{-1}) in the tropical Pacific (110°E–75°W, 26°S–26°N) in response to a uniform 2°C increase in SST. (c) As in (b) except for changes in relative humidity (%) vs changes in surface evaporation expressed as latent heat flux (W m^{-2}).

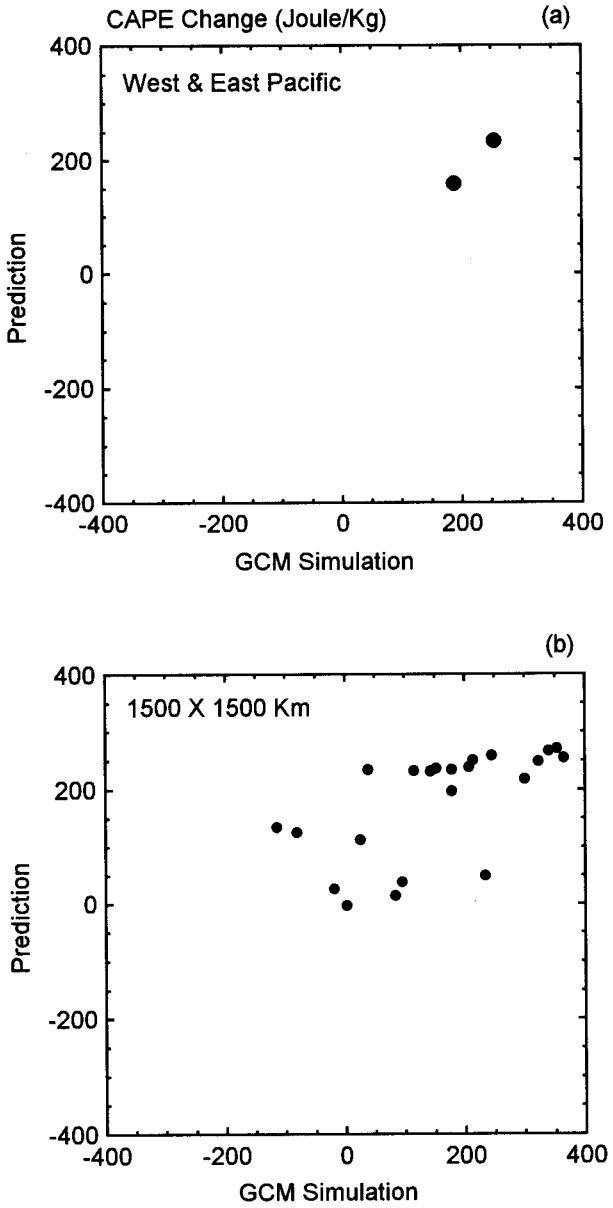

FIG. 11. Scatterplots of predicted changes in CAPE (J kg^{-1}) vs simulated changes in CAPE on two different spatial scales: (a) the tropical Pacific is divided into the western (110°E–170°W) and eastern (170°–90°W) Pacific; (b) on the scale of 12° × 15°.

tal scales from the original gridpoint profiles obtained from the GCM. Table 2 shows that the predicted CAPE change averaged over the tropical Pacific agrees closely with the simulation by the GCM; the prediction is only slightly smaller for reasons we have addressed before. This suggests that climate changes in the Hadley and Walker cells have little effect on the mean conditional instability over their entire domain. In Fig. 11a, the tropical Pacific (110°E–90°W, 22°S–22°N) is further divided into the western (110°E–170°W) and eastern (170°–90°W) Pacific, and CAPE changes calculated in

each part of the ocean are found to agree well with the simulated values. Given that the prediction is good at the largest scales but is poor at scales of about 500 km (see Fig. 9a), a typical scale of larger cloud clusters, it is interesting to determine the scale at which the transition in prediction accuracy occurs. Figure 11b shows a scatterplot of predicted versus realized CAPE change on scales of 1500 km, approximately the equatorial Rossby radius of deformation and a characteristic scale for the growth of tropical easterly waves. On this scale there is significant scatter, but a correlation between predicted and realized CAPE change is still evident. This suggests that if one wants to predict the change in convective instability on synoptic or smaller scales in a warmer climate, it is necessary to know how the tropical wave characteristics change—for example, frequency, wavelength, track, and transports of heat and moisture.

To this point, we have examined an idealized warmer climate with uniformly increased SST; however, there are several reasons to believe that the rise of SST in a climate change may not be longitudinally symmetric. 1) The west Pacific may warm less than the east Pacific because deep convective clouds and their associated anvils over the warm pool have higher albedo and reflect more solar radiation to cool the surface (Ramanathan and Collins 1991). 2) The ocean mixed layer becomes shallower as one moves eastward across the tropical Pacific, implying a shorter response time and thus larger transient response to climate forcings in the east Pacific. 3) Increases in surface evaporative cooling may be greater in the warm pool (Knutson and Manabe 1995). 4) The drier east Pacific boundary layer may experience a larger increase in downward longwave flux than the more opaque west Pacific boundary layer. On the other hand, ocean models coupled to simple atmospheres suggest that increased cooling by east Pacific Ocean upwelling may increase the longitudinal SST gradient instead (Clement et al. 1996). The change of the large-scale circulations in different scenarios of SST change are expected to be quite different since longitudinal circulations are thermally driven by the SST gradient (Lindzen and Nigam 1987). To see whether the results on climate change presented previously are dependent on changes in SST patterns, we conducted a sensitivity test to partially simulate these effects. For simplicity, SST outside the tropical Pacific was set to be uniformly 2°C higher or lower, but inside the SST was modified unevenly at each latitude (Φ) and longitude (λ) according to the following parameterization:

$$d\mathrm{SST}(\lambda, \Phi) = [\mathrm{SST}_{\max}(\Phi) - \mathrm{SST}(\lambda, \Phi)]\alpha, \quad (8)$$

where $\mathrm{SST}_{\max}$ is the maximum SST at a given latitude across the Pacific. The magnitude of the perturbation in SST given by (8) is proportional to the difference relative to the maximum SST at the same latitude, so that the longitudinal SST gradient is weakened in the SST +2 experiment but strengthened in the SST −2 experiment. The coefficient α is determined by the closure assumption that the mean SST change averaged over each latitude in the tropical Pacific is ±2°C, which is the same as outside the tropical Pacific. This makes the zonal mean meridional SST gradient independent on how the SST within the region of interest is modified. Figure 12 shows the resulting SST distributions for the warmer climate assuming uniform and nonuniform perturbations; it is obvious that the strong gradient of SST from west to east has been greatly reduced in the latter scenario.

The effects of the weakened SST gradient on the circulation field are shown in Fig. 13a. Relative to the current climate regime with strong zonal SST gradient, there is a westerly/easterly anomaly in the lower-upper-tropospheric wind field associated with the weaker SST gradient. The weaker Walker circulation also affects the boundary layer moisture field. Comparing the spatial distribution of relative humidity and surface convergence (Figs. 13b,c), we find that in areas with SST > 27°–28°C, regions with decreasing relative humidity correlate fairly well with decreasing surface convergence. The negative relative humidity change in the cooler eastern Pacific, despite increased convergence in part of the region, is mainly caused by the weakened surface wind, which suppresses the increase of surface evaporation, so that specific humidity increases less than the imposed increase in saturation specific humidity. The weaker surface convergence on either side of the equator is probably a result of the weaker Walker circulation in the intertropical and South Pacific convergence zones in response to a weaker longitudinal SST gradient. The different regional pattern of relative humidity change (relative to the uniform SST +2 case) results in different local CAPE changes, but averaged over the basin, the CAPE change is only slightly smaller than that for a uniform increase in SST (Table 2a). The weakened west Pacific moisture convergence in the reduced gradient scenario has a larger effect on the radiative properties of parameterized cumulus anvils, resulting in significantly higher climate sensitivity of top-of-the-atmosphere radiative fluxes (Del Genio et al. 1996).

The effect of SST pattern on CAPE is another example of differences between warm and cold climate perturbations. For a 2°C SST decrease, a scenario with strengthened SST gradient exhibits a much smaller CAPE change than a scenario of uniform cooling (Table 2b).

5. Discussion

Since the climate sensitivity of CAPE to surface temperature is only about 50–100 J kg^{-1} $^{\circ}\mathrm{C}^{-1}$, an order of magnitude smaller than the observed sensitivity to variations in the current climate, it is not obvious that the small anthropogenic greenhouse signal in surface temperature will be magnified by the lightning rate suffi-

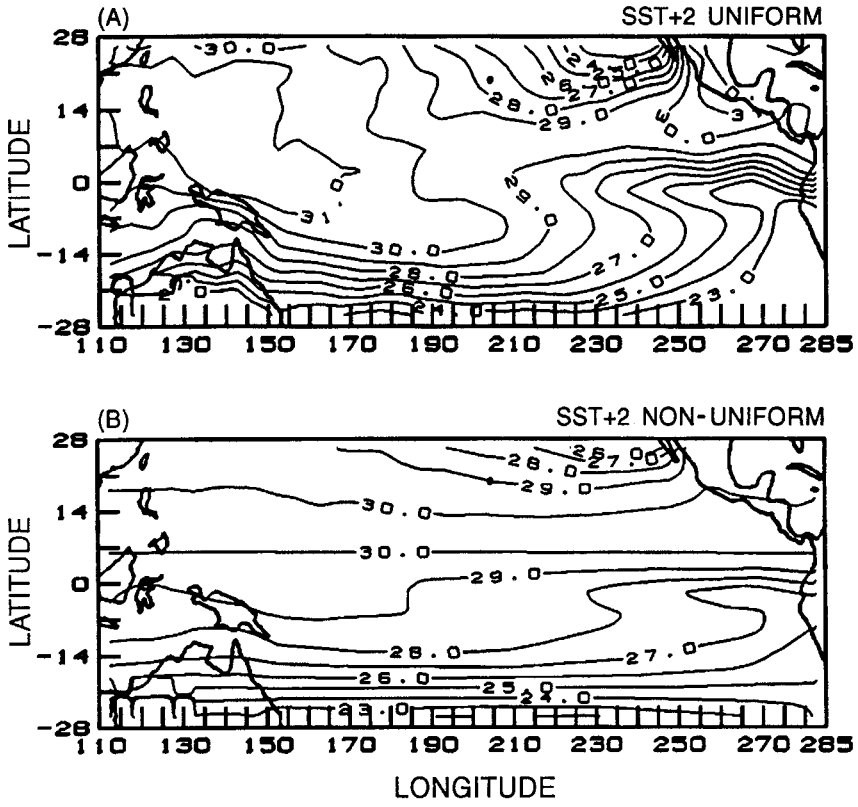

FIG. 12. Geographical distributions of tropical Pacific SST (°C) for July for (a) a uniform 2°C increase in SST and (b) a nonuniform 2°C increase in SST specified to weaken the longitudinal gradient.

ciently to be detected in the global electrical circuit (Williams 1992). The reported correlation between the tropical average temperature and the magnetic field on a timescale of several years (Williams 1992) may not be properly applied to a multidecadal externally forced climate change for the following reason: Interannual variations of SST are not communicated efficiently to higher levels; at and above the trade inversion, vertical motions associated with tropical circulation anomalies offset the effects of convective heating anomalies and reduce thermodynamic structure changes there (Garcia et al. 1986; Fu et al. 1996). On the other hand, long-term forced climate changes drive the atmosphere toward a new radiative–convective equilibrium in which the Hadley and Walker cell changes (as simulated by the GCM) are much weaker, so that an increase in convection warms upper levels more than lower levels, limiting CAPE change. However, lightning occurrence is a very nonlinear function of convection intensity. Solomon and Baker (1994) report a reversibly defined threshold CAPE for lightning occurrence of about 400 J kg^{-1}. The GISS GCM simulation suggests that in the current climate more than 50% of tropical Pacific grid points have a reversibly defined CAPE around 300 J kg^{-1}. If 100 J kg^{-1} of CAPE due to a 2°C increase in SST is added to that for the current climate, then the barrier for the occurrence of lightning can more frequently be overcome to induce a jump in lightning frequency. Over tropical oceans, the strongest 10% of cumulus updrafts have a vertical velocity of at least 4 m s^{-1}, and the threshold cumulus updraft velocity W for lightning has been suggested to be 6–12 m s^{-1} (Zipser and Lutz 1994). If we assume as an upper limit that CAPE increase in a warmer climate is effectively converted into kinetic energy according to $W = (2\text{CAPE})^{1/2}$, a 2°C increase in SST implies a 4 m s^{-1} increase in the cumulus updraft velocity, which barely satisfies the required additional kinetic energy to trigger lightning activity. However, observed updraft speeds are substantially less than the maximum theoretical value indicated by observed values of CAPE; other factors such as the shape of the buoyancy profile, boundary layer depth, degree of convective inhibition near the surface, and water loading may also affect updraft intensity (Lucas et al. 1994a). It is therefore difficult to conclude that increased lightning will necessarily accompany global warming.

If the finite increase of CAPE in a warmer climate produces stronger convective updrafts, this change has several climatic implications. More water vapor or condensate might be transported upward and eventually detrained to form large-scale stratiform clouds, which have

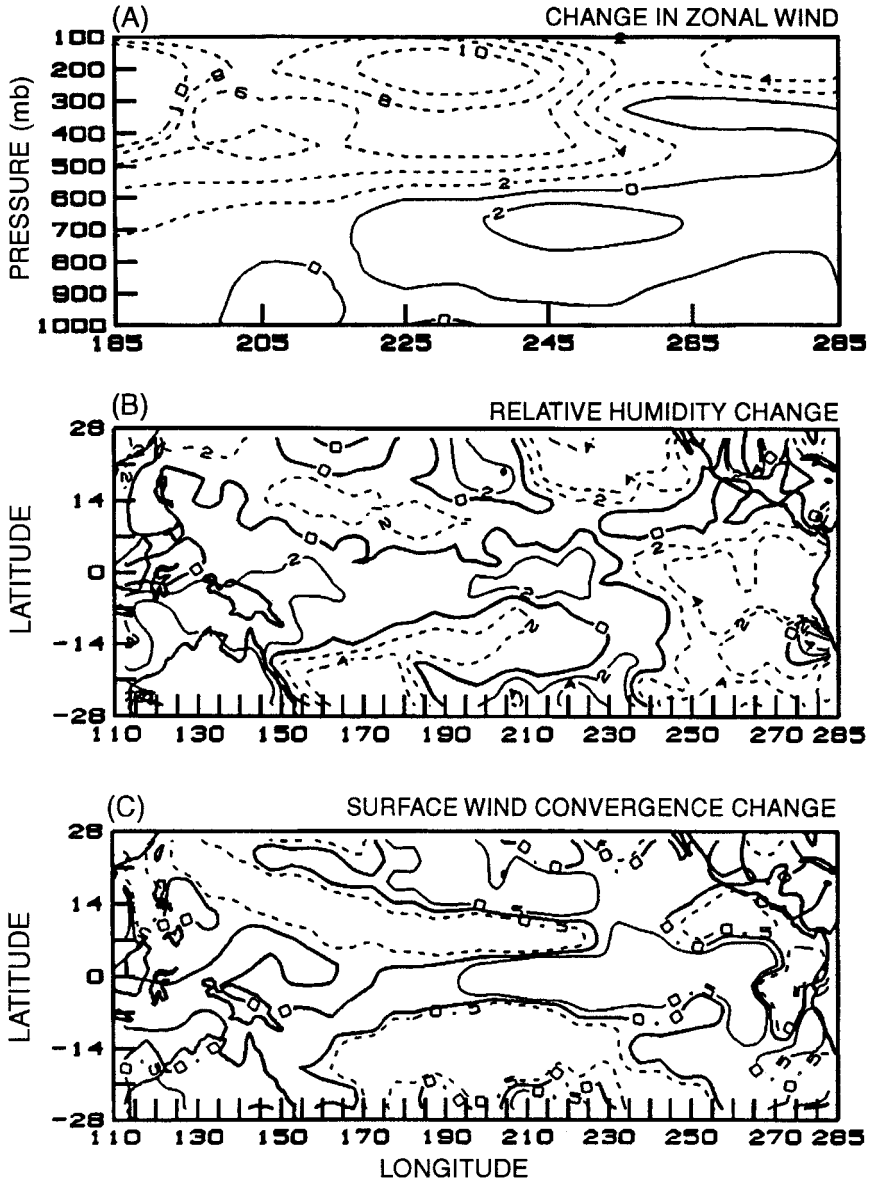

FIG. 13. (a) Change in the vertical–longitudinal distribution of zonal wind (m s^{-1}) in the southeastern tropical Pacific (175°–75°W, 0°–6°S) in response to a nonuniform 2°C increase in SST. (b) Geographical distribution of the change in surface relative humidity (%) in response to a nonuniform 2°C increase in SST. (c) As in (b) but for surface convergence (10^{-6} s^{-1}).

large impacts on the radiation budget because of their large horizontal cover and optical thickness. The evaporation of anvil clouds adds more water vapor to the upper troposphere to enhance the clear-sky greenhouse effect. Some convective updrafts will detrain at higher, colder levels to form cirrus clouds with greater longwave cloud forcing.

However, whether the net vertical transport of moisture by convection increases or not in a warmer climate depends not only on the change of cumulus updraft intensity but also on the changes in the fractional area covered by active convection and in the vertical moisture gradient because the moisture flux is proportional to the product of all three parameters. Futhermore, the net flux also depends on changes in the sedimentation velocities of precipitation drops relative to the change in updraft speed. In one possible scenario, even with more intense cumulus updrafts in a warmer climate, the more efficient release of latent heat and greater capability of cumulus convection to remove conditional instability might lead to a smaller convective area. If this tendency dominates that due to the increased updraft velocity, or if raindrop fall speeds increase more than the updraft velocity, then the moisture transport by con-

vection could conceivably remain unchanged or even decrease. In the GISS GCM, the fractional area of convection is not predicted, but the cumulus mass flux—which is proportional to the product of vertical velocity and fractional area—is. The SST +2 climate change experiments suggest an increase in deep cumulus mass flux. The climate change experiments also indicate an increase in the vertical moisture gradient (Del Genio et al. 1991), which is consistent with the strong constraint provided by the Clausius–Clapeyron equation. The net result implied by the GISS GCM is that the more vigorous moist convection will enhance vertical moisture exchange between the PBL and the upper troposphere if the climate becomes warmer in the future. Below the detrainment level, the increased cumulus mass flux and moisture gradient produce increased cumulus subsidence drying instead, although this is offset by increased large-scale vertical advection to produce net moistening at all levels.

In addition to the change in moisture budget caused by cumulus convection in the upper troposphere, microphysical conditions and cloud radiative properties at middle and upper levels may also be subject to the change in CAPE because of the possible increase of moisture source discussed above. In addition, the enhanced ability of stronger cumulus updrafts to vertically advect larger cloud droplets with higher terminal velocities may cause the particle size distribution and the number density of cloud droplets to be different from those in the current climate. This is important because GISS GCM simulations indicate that changes in tropical anvil clouds control the model's climate sensitivity (Del Genio et al. 1996).

If we assume for illustrative purposes that the shape of the size distribution and the effective radius do not change as CAPE changes in a warming climate, then all the increased moisture goes to increase the number density of cloud droplets. Cloud optical thickness τ is related to cloud water content μ and effective radius r_e according to

$$\tau \approx 3\mu\Delta z/2\rho r_e \tag{9}$$

(Hansen and Travis 1974), where Δz is the physical thickness of the cloud and ρ is the density of liquid water. If we neglect the climatic variation of Δz, (9) implies that τ varies linearly with μ. If we further assume for simplicity that the cloud water content μ is a linear function of cumulus updraft velocity, then the 10% increase in vertical velocity derived from the 200 J kg^{-1} increase in CAPE implies a similar fractional change of optical thickness. For anvil clouds with optical thickness $\tau \sim 20$, a 10% increase implies $\Delta\tau \sim 2$. On the other hand, if we assume that the number density of cloud particles does not change in the future climate, then the extra moisture is used instead to enlarge cloud droplets. Since $r_e \propto \mu^{1/3}$ if number density is constant, Eq. (9) then implies that the fractional change of optical thickness τ is two-thirds the fractional change of μ and thus vertical velocity. The corresponding absolute change of τ for anvil clouds is thus 1.3. According to studies of the sensitivity of radiation budget to cloud properties (Zhang et al. 1995; Rossow et al. 1995), the corresponding net change in mean radiation balance (Solar + IR) for $\Delta\tau \sim 1.3$–2.0 would be 4.3–6.7 W m^{-2}, which is comparable in magnitude to the 4 W m^{-2} caused by a doubling of CO_2.

The real world situation may fall between these two simple extremes with the number density of cloud droplets, shape of the size distribution, and the effective mean radius all changing simultaneously. Furthermore, the relationship between changes in updraft speed and changes in detrainment of convective condensate is a complex microphysical problem unlikely to exhibit the simple linear behavior we have assumed in this example. However, the calculations presented above give us a crude estimate of the potential climate signal for such changes and demonstrate that predicting the change in CAPE and thus cumulus activity is important not only for the hydrological cycle but also for cloud feedback and overall climate sensitivity to external perturbations. The example presented here suggests that a realistic parameterization of the dependence of condensate detrainment on cumulus updraft intensity is among the most important challenges for future climate GCM development.

Acknowledgments. We thank two anonymous reviewers for their thoughtful suggestions that improved the paper. We also appreciate Lilly Del Valle's assistance in making the figures used in this paper. This research was supported by the NASA Tropical Rainfall Measuring Mission, the First ISCCP Regional Experiment III, the DOE Atmospheric Radiation Measurement Program, and the Earth Observing System Interdisciplinary Research Program.

REFERENCES

Arakawa, A., and W. H. Schubert, 1974: Interaction of a cumulus cloud ensemble with the large-scale environment. Part I. *J. Atmos. Sci.,* **31,** 674–701.

Betts, A. K., 1982: Saturation point analysis of moist convective overturning. *J. Atmos. Sci.,* **39,** 1484–1505.

——, and W. Ridgway, 1989: Climatic equilibrium of the atmospheric convective boundary layer over a tropical ocean. *J. Atmos. Sci.,* **46,** 2621–2641.

Brown, R. G., and C. S. Bretherton, 1997: A test of the strict quasi-equilibrium theory on long time and space scales. *J. Atmos. Sci.,* **54,** 624–638.

Clement, A. C., R. Seager, M. A. Cane, and S. E. Zebiak, 1996: An ocean dynamical thermostat. *J. Climate,* **9,** 2190–2196.

Del Genio, A. D., 1993: Convective and large-scale cloud processes in GCMs. *Energy and Water Cycles in the Climate System,* E. Raschke and D. Jacob, Eds., NATO ASI Series, Vol. 15, Springer-Verlag, 95–121.

——, and M.-S. Yao, 1988: Sensitivity of a global climate model to the specification of convective updraft and downdraft mass fluxes. *J. Atmos. Sci.,* **45,** 2641–2668.

——, and ——, 1993: Efficient cumulus parameterization for long-term climate studies: The GISS scheme. *The Representation of*

Cumulus Convection in Numerical Models, Meteor. Monogr., No. 46, Amer. Meteor. Soc., 181–184.

——, A. A. Lacis, and R. A. Ruedy, 1991: Simulations of the effect of a warmer climate on atmospheric humidity. *Nature,* **351,** 382–385.

——, M.-S. Yao, W. Kovari, and Kenneth K.-W. Lo, 1996: A prognostic cloud water parameterization for global climate models. *J. Climate,* **9,** 270–304.

Fitzjarrald, D. R., and M. Garstang, 1981: Boundary-layer growth over the tropical ocean. *Mon. Wea. Rev.,* **109,** 1762–1772.

Fu, R., 1991: Deep convection and its relation to the large-scale circulation in the tropical Pacific. Ph.D. dissertation, Columbia University, 166 pp.

——, A. D. Del Genio, and W. B. Rossow, 1994: Influence of ocean surface conditions on atmospheric vertical thermodynamic structure and deep convection. *J. Climate,* **7,** 1092–1108.

——, W. T. Liu, and R. E. Dickinson, 1996: Response of tropical clouds to the interannual variation of sea surface temperature. *J. Climate,* **9,** 616–634.

Garcia, O., S. J. S. Khalsa, and E. J. Steiner, 1986: Atmospheric characteristics of the equatorial Pacific during the 1982–1983 El Niño, deduced from satellite and aircraft observations. *J. Geophys. Res.,* **91,** 13 217–13 231.

Gill, A. E., 1980: Some simple solutions for heat-induced tropical circulation. *Quart. J. Roy. Meteor. Soc.,* **106,** 447–462.

Hansen, J., and L. Travis, 1974: Light scattering in planetary atmospheres. *Space Sci. Rev.,* **16,** 527–610.

——, G. Russell, D. Rind, P. Stone, A. Lacis, S. Lebedeff, R. Ruedy, and L. Travis, 1983: Efficient three-dimensional global models for climate studies: Models I and II. *Mon. Wea. Rev.,* **111,** 609–662.

Knutson, T. R., and S. Manabe, 1995: Time-mean response over the tropical Pacific to increased CO_2 in a coupled ocean–atmosphere model. *J. Climate,* **8,** 2181–2199.

Lindzen, R. S., and S. Nigam, 1987: On the role of sea surface temperature gradients on forcing low level winds and convergence in the Tropics. *J. Atmos. Sci.,* **44,** 2440–2448.

Lucas, C., E. J. Zipser, and M. A. LeMone, 1994a: Vertical velocity in oceanic convection off tropical Australia. *J. Atmos. Sci.,* **51,** 3183–3193.

——, ——, and ——, 1994b: Convective available potential energy in the environment of oceanic and continental clouds: Correction and comments. *J. Atmos. Sci.,* **51,** 3829–3830.

Manabe, S., J. Smagorinsky, and R. F. Strickler, 1965: Simulated climatology of a general circulation model with a hydrologic cycle. *Mon. Wea. Rev.,* **93,** 769–798.

Oort, A. H., 1983: Global atmospheric circulation statistics, 1958–1973. NOAA Professional Paper 14, 180 pp.

Ramanathan, V., and W. Collins, 1991: Thermodynamic regulation of ocean warming by cirrus clouds deduced from observations of the 1987 El Niño. *Nature,* **351,** 27–32.

Rind, D., E. W. Chiou, W. Chu, J. Larsen, S. Oltmans, J. Lerner, M. P. McCormick, and L. McMaster, 1991: Positive water vapor feedback in climate models confirmed by satellite data. *Nature,* **349,** 500–503.

Rossow, W. B., and B. Cairns, 1995: Monitoring changes of clouds. *Climate Change,* **31,** 175–217.

Solomon, R., and M. Baker, 1994: Electrification of New Mexico thunderstorms. *Mon. Wea. Rev.,* **122,** 1878–1886.

Thompson, R. M., Jr., S. W. Payne, E. E. Recker, and R. J. Reed, 1979: Structure and properties of synoptic-scale wave disturbances in the intertropical convergence zone of the eastern Atlantic. *J. Atmos. Sci.,* **36,** 53–72.

Williams, E., 1992: The Schumann resonance: A global tropical thermometer. *Science,* **256,** 1184–1187.

——, 1994: Global circuit response to seasonal variations in global surface air temperature. *Mon. Wea. Rev.,* **122,** 1917–1929.

——, and N. Renno, 1993: An analysis of the conditional instability of the tropical atmosphere. *Mon. Wea. Rev.,* **121,** 21–36.

Xu, K. M., and K. A. Emanuel, 1989: Is the tropical atmosphere conditionally unstable? *Mon. Wea. Rev.,* **117,** 1471–1479.

Yanai, M., S. Esbensen, and J. Chu, 1973: Determination of bulk properties of tropical cloud clusters from large-scale heat and moisture budget. *J. Atmos. Sci.,* **30,** 611–627.

Yao, M.-S., and A. D. Del Genio, 1989: Effects of cumulus entrainment and multiple cloud types on a January global climate model simulation. *J. Climate,* **2,** 850–863.

Zhang, Y.-C., W. B. Rossow, and A. A. Lacis, 1995: Calculation of surface and top-of-atmosphere radiative fluxes from physical quantities based on ISCCP datasets. Part 1: Method and sensitivity to input data uncertainties. *J. Geophys. Res.,* **100,** 1149–1165.

Zipser, E. J., and K. R. Lutz, 1994: The vertical profile of radar reflectivity of convective cells: A strong indicator of storm intensity and lightning probability? *Mon. Wea. Rev.,* **122,** 1751–1759.